Research Article

The determination of *Plutella xylostella* (L.) GSTs (PxGSTs) involved in the detoxification metabolism of Tolfenpyrad

Yifan Li,[a] Hong Sun,[a] Zhen Tian,[b] Xinxin Su,[a] Yue Li,[a] Xuan Ye,[a] Yifei Zhou,[a] Shengli Zheng,[c] Jiyuan Liu[a]* and Yalin Zhang[a]*

Abstract

BACKGROUND: Insect glutathione S-transferases (GSTs) play a crucial role in insecticide detoxification. However, there remains a distinct lack of information regarding the role of GSTs in the detoxification of Tolfenpyrad (TFP) in insects.

RESULTS: Real-time quantitative PCR showed significant upregulation of PxGSTs after exposure to TFP for 6 h. An *in vitro* inhibition assay showed that TFP could inhibit PxGSTδ, PxGSTε and PxGSTσ, and the most pronounced inhibitory effect was on PxGSTσ. Metabolism assays displayed that PxGSTσ was superior to other test PxGSTs in metabolizing TFP. The molecular docking of TFP and PxGSTσ revealed that the H-bond provided by the sidechains of Tyr107 and Tyr162 were key to the detoxification of TFP by PxGSTσ. Further tests using mutant PxGSTσ proteins at the sites of Tyr107 (PxGSTσY107A) and Tyr162 (PxGSTσY162A) corroborated that the individual replacement of Tyr107 and Tyr162 could greatly weaken the binding and metabolic abilities to TFP.

CONCLUSION: Metabolic interactions between the *Plutella xylostella* (L.) GSTs (PxGSTs) and TFP were deciphered. This study illustrates the molecular metabolism mechanism of PxGSTσ towards TFP and provides theoretical underpinnings for the design and optimization of novel TFP-like insecticides.
© 2020 Society of Chemical Industry

Supporting information may be found in the online version of this article.

Keywords: glutathione S-transferases (GSTs); Tolfenpyrad (TFP); molecular docking; site-directed mutagenesis; *Plutella xylostella*

1 INTRODUCTION

The diamondback moth, *Plutella xylostella* (L.) (Lepidoptera: Plutellidae) is one of the most destructive pests of cruciferous plants in the world.[1,2] The annual cost of controlling *P. xylostella* has reached billions of dollars.[3–6] Presently, chemical control is the most effective measure to prevent *P. xylostella*.[7] However, *P. xylostella* has developed resistance to most commonly used commercial pesticides including organophosphates, organochlorines, pyrethroids and carbamates.[8] Therefore, it is of importance to maintain the control effect of insecticides on *P. xylostella* and to design new insecticidal components for the control of *P. xylostella*.

Tolfenpyrad (TFP) is a mitochondrial complex I inhibitor with pronounced insecticidal activity against Hemiptera, Coleoptera, Diptera, Lepidoptera, Thysanoptera and Acarina pests.[9,10] Furthermore, it has been documented that TFP has a high insecticidal activity against *P. xylostella*.[11] However, studies have indicated that the risk of developing resistance to TFP is relatively high in *P. xylostella*.[12] Meanwhile, it has been found that *P. xylostella* has developed high levels of resistance to TFP in Asia.[13] Despite these reports of TFP resistance in *P. xylostella*, the mechanism involved in the development of this resistance remains elusive.

The enhancement of detoxification enzymes metabolism is a crucial part in the mechanism of insecticide resistance.[14,15] As a phase-II detoxification enzyme, glutathione S-transferases (GSTs) are important in metabolizing endogenous compounds and xenobiotics.[16,17] GSTs catalyze the conjugation of reduced glutathione (GSH) with xenobiotics, making the conjugated compounds soluble and enabling detoxification through excretion.[18,19] To date, insect GSTs have been reported to be involved in resistance to organophosphates, pyrethroids and the acaricide cyflumetofen.[20–23] Insect cytosolic GSTs are classified into six families: δ, ε, σ, ω, θ and ζ. Among them, δ and ε are specific to insects.[24,25] The published *P. xylostella* genome database (PDB) identifies 22 cytosolic GSTs, classified mainly into the

* *Correspondence to: Y Zhang or J Liu, Key Laboratory of Plant Protection Resources & Pest Management of the Ministry of Education, College of Plant Protection, Northwest A&F University, Yangling, Shaanxi 712100, China, E-mail: yalinzh@nwsuaf.edu.cn (Zhang); E-mail: kingljy0818@hotmail.com (Liu)*

† *Yifan Li, Hong Sun and Zhen Tian should be considered joint first authors.*

a   *Key Laboratory of Plant Protection Resources & Pest Management of the Ministry of Education, College of Plant Protection, Northwest A&F University, Yangling, China*

b   *College of Horticulture and Plant Protection, Yangzhou University, Yangzhou, China*

c   *College of Chemistry & Pharmacy, Northwest A&F University, Yangling, China*

six families described previously.[26] According to previously reported statistics, of the known PxGSTs classes, only δ, ε and σ can find templates with >45% homology in PDB.[27] Additionally, current research has emphasized that δ, σ and ε classes of GSTs are the major GSTs used to detoxify insecticides by insects.[28–31]

In this study, we report the function of PxGSTδ, PxGSTσ and PxGSTε in the detoxification of TFP. Our study deciphers the binding modes of PxGSTσ–TFP interaction and verifies the key amino acid sites of PxGSTσ in metabolizing TFP.

2 MATERIALS AND METHODS

2.1 Insects
The susceptible *P. xylostella* population was provided by the Key Lab of Plant Protection Resources & Pest Management of the Ministry of Education, Northwest A&F University, Yangling, China. They have been reared in indoor conditions for over 10 years without being exposed to any insecticides (25 ± 2 °C, 50 ± 5% relative humidity with a photoperiod of 16 h:8 h, light:dark). The larvae were raised on cabbage (*Brassica oleracea*) which had been maintained in the laboratory without being exposed to any insecticides. Adults were supplied with 10% insecticide-free honey water.

2.2 Chemicals
Imidacloprid, thiamethoxam, rotenone, halofenozide, tolfenpyrad, (E)-fenpyroximate, chlorantraniliprole and diflubenzuron (technical grade: purity>98%) were purchased from Topscience (Shanghai, China). Reduced GSH(purity>98%) and 1-chloro-2,4-dinitrobenzene (CDNB, purity>98%) were obtained from Aladdin (Shanghai, China). All other chemicals or reagents were reagent grade.

2.3 Bioassay
The TFP was diluted using 50% acetone-water mixture to eight concentrations (1, 2, 4, 8, 16, 32, 64 and 128 mg L^{-1}). The control group was treated with a 50% acetone-water mixture. Leaves of *B. oleracea* (radius $\approx$ 2 cm) were soaked in the solutions using a leaf-dipping method for 2–3 s.[32] The soaked leaves were dried until the acetone volatilized in a fume hood. The leaves then were put into petri dishes with moisturizing filter paper covering the bottom. New leaves were supplied daily in order to maintain sufficient leaves to feed larvae. Every dish was supplied with ten 3rd instar larvae for experiments. They were maintained under the conditions described previously and each treatment was repeated three times. Larvae would be considered dead if they were unable to move after soft prodding with a fine brush. Mortality rates were recorded at 24 h, 48 h and 72 h. The mortality of the control group was corrected by Abbott's correction to ensure a control mortality lower than 15%.[33] Data were subjected to Probit analysis using SPSS 19.0 software (IBM, USA) to obtain maxiumum doses for 10, 50 and 90% mortality (LC$_{10}$, LC$_{50}$ and LC$_{90}$ values, respectively), and chi-squared (χ^2).

2.4 Insecticide exposure
The bioassay data were analyzed to determine the LC$_{10}$, LC$_{50}$ and LC$_{90}$ of TFP against *P. xylostella* at 24, 48 and 72 h. The LC$_{10}$ concentration of the TFP bioassay at 48 h was employed in the insecticide exposure experiments. Control groups were treated with acetone. The larvae were treated following the bioassay method mentioned previously. Three replicates were set for each experiment. Larvae were sampled at 3, 6, 12, 24 and 48 h with ten surviving larvae taken each time. Subsequently, the larvae were flash-frozen in liquid nitrogen and stored at −80 °C before transcription analysis.

2.5 Quantitative reverse transcription polymerase chain reaction (qRT-PCR)
In order to determine the expression levels of PxGSTδ (PxGSTδ1, GenBank: AB541016.1), PxGSTε (PxGSTε3, GenBank: U66342.1) and PxGSTσ (PxGSTσ2, GenBank: AB180454.1) responding to TFP exposure at different times, qRT-PCR was conducted using the primers in Table S1, which was designed by Integrated DNA Technologies (IDT) primer quest tool (https://sg.idtdna.com/PrimerQuest/Home/Index). *Elongation factor 1* (*EF-1*) (GenBank: EF417849.1) and *ribosomal protein L32* (*RPL32*) (GenBank: AB180441.1) were chosen to be the internal reference genes which have been reported before.[34] The synthesis of cDNA used TransScript® one-step gDNA removal and cDNA synthesis SuperMix (TransGen, China) according to the manufacturer's instructions. Components of qRT-PCR were added by using TransStart® tip green qPCR SuperMix (TransGen) in terms of the manufacturer's instructions. This process was performed in LightCycler®480 (Roche, Swiss). The amplification procedure was performed by the Two-step method which was started at 94 °C for 5 min, followed by 45 cycles consisting of 94 °C for 5 s and 56 °C for 30 s. Afterwards, a melting curve was automatically generated to confirm the specificity of PCR products. The obtained PCR products were subjected to 1% agarose gel electrophoresis detection (Fig. S4). Negative controls used RNase-free water to take the place of the cDNA template. A serial ten-fold dilution of cDNA temple was used to establish a standard curve to determine the amplification efficiency. The amplification efficiency (*E*) was calculated following the equation $E = \left(10^{\left[-\frac{1}{\text{slope}}\right]}\right) \times 100$. Each PCR reaction was conducted with three biological and technique replications. Statistics were calculated based on 2$^{-\Delta\Delta Ct.}$ method.[35] The fold-increase was derived from the expression level of PxGSTs in the insecticide-treated group divided by the acetone-treated control, and the ratio was used for expression profile analysis. The expression levels of PaGSTs were analyzed using one-way ANOVA, using Prism 6 (GraphPad Software, Inc., La Jolla, CA, USA), followed by Tukey's multiple comparisions test to evaluate significant differences. Results were displayed as means ± SE.

2.6 Binding mode analysis
The ligand TFP was docked into the binding cavity of PxGSTσ by the program GOLD 5.3.[36,37] The 3D structure of PxGSTσ that we used for molecular docking was the model constructed in our former research.[27] The 3D PxGSTσ model was further run for 5000 steps to conduct energy minimization in Amber12 with the ff99SB force field.[38,39] The 3D structure of TFP was sketched using Maestro version (Version 10.1, Schrodinger Inc., USA) and optimized for 2000 steps in Amber12 with the GAFF force field.[38,40] In the process of docking simulations, the C3 atom coordinate derived from the PxGSTσ-GTX complex in our previous research was defined as the centroid of the binding site with a 10 Å radius sphere.[27] ChemPLP score, which was superior to other scoring functions in GOLD for pose prediction,[41,42] was employed to predict the most accurate binding modes for TFP. The pharmacophore model and the interaction diagram were presented by LigandScout 4.4.1.[43] Visualization of the structures was performed by PyMol 1.3r1.[44]

2.7 Binding energy calculations

In order to investigate the binding affinity between TFP and PxGSTσ, the docking pose for TFP with the highest ChemPLP score was re-scored by Chemscore.[45,46] The Chemscore delta value calculated using the Chemscore function was applied to measure the PxGSTσ–TFP affinity.[23,42] Chemscore estimates the binding free energy ΔG according to Eqn (1):

$$\Delta G_{binding} = \Delta G_O + \Delta G_{hbond} + \Delta G_{lipo} + \Delta G_{rot} \quad (1)$$

The Chemscore function in our work can be written in the form:

$$\Delta G = -5.4800 + -3.3400 * S\,(hbond) + -0.1170 * S\,(lipo) \\ + 2.5600 * H\,(rot) \quad (2)$$

Each component of this equation is the product of a term depending on the magnitude of a particular physical contribution to free energy (e.g. hydrogen bonding).

2.8 Gene synthesis and site-directed mutagenesis

Sequences of PxGSTδ (PxGSTδ1, GenBank: AB541016.1), PxGSTε (PxGSTε3, GenBank: U66342.1) and PxGSTσ (PxGSTσ2, GenBank: AB180454.1) containing restriction enzyme sites *Nde*I and *Hind*III were synthesized by Sangon Biotech (Shanghai, China). Site-directed mutagenesis was conducted following the protocol of *Fast Mutagenesis* System (cat. no. FM111-01, TransGen). The primers for site-directed mutagenesis were designed in terms of the instructions of the *Fast Mutagenesis* System.

2.9 Expression and purification of recombinant native and mutant GST proteins *in vitro*

These native PxGSTs genes were ligated into the *pET-30a* (+) vector to construct the expression vector *pET-30a-GSTs*. After that, the recombinant vectors were transformed into competent BL21 (DE3) cells to express GSTs. Then, the BL21 (DE3) cells harboring the recombinant vectors were cultured on LB (1 L) medium containing kanamycin(50 mg mL^{-1}) and incubated overnight at 37 °C. Isopropyl β-D-1-thiogalactopyranoside (IPTG) was added to the LB medium with a final concentration of 0.4 mM when the OD$_{600}$ reached 0.6 and induced overnight at 30 °C and 200 rpm. The recombinant cells were collected by centrifugation at 10 000×g, 4 °C for 10 min. The supernatant was resuspended in 10 mL PBS (10 mM, pH 7.4) and lysed by sonicating with 250 W for 10 min (work 10 s/ stop 10 s intervals) on ice (Sonics & Materials Inc., Newtown, CT, USA). The resulting cell pellet was collected after centrifugation at 8000×g, 4 °C for 20 min. For purification, the cell pellet was added to the Ni-NTA (YEASEN, China) column. The recombinant protein was subjected to a gradient elution using 50 mM, 100 mM, 150 mM, 200 mM, 250 mM and 500 mM imidazole. The target proteins were detected using 12% SDS-PAGE and were dialyzed using PBS (10 mM, pH 7.4) overnight. The determination of the protein concentration was followed by the BCA Protein Assay Kit (Leagene, China). The method for expression and purification of recombinant mutant proteins was identical to the native PxGSTs.

2.10 Kinetics of recombinant PxGSTs

In order to measure the enzymatic kinetics of purified PxGSTs, a 200-μL volume reaction mixture consisting of 1 μg PxGSTs protein, different concentrations of CDNB (0.05, 0.1, 0.2,0.4, 0.8 and 1.6 mM) and 1 mM GSH (dissolved in 0.1 M sodium phosphate buffer) were added into the transparent 96-well plates. Reactions were detected by using infinite M200 Microplate Reader (Tecan, Switzerland) at 340 nm (A340) for 5 min at 25 °C (kinetic cycle six times, each interval 1 min). The acquired changes of absorption were transformed into CDNB conjugated per min per mg protein based on the extinction coefficient of 9600 M^{-1} cm^{-1}. Data were imported into Prism 6.0 software (GraphPad) to calculate the kinetics parameters (V_m and K_m) by the Michaelis–Menten plot; each plotted point represented triple measurements.

2.11 Assays on inhibition of recombinant PxGSTs protein by insecticides

The inhibition assays were conducted following a previously reported method with slight optimization.[47] Specifically, the pre-incubation mixtures including 1 μg recombinant GSTs protein, 2 μL appropriately diluted insecticides (imidacloprid, thiamethoxam, rotenone, halofenozide, tolfenpyrad, (E)-fenpyroximate, chlorantraniliprole and diflubenzuron), 2 μL CDNB (1 mM) and 100 μL PBS (100 mM) buffer were mixed and incubated at 25 °C for 10 min. After incubation, a final concentration of 1 mM GSH and 1 mM CDNB were added sequentially into the mixtures to start the reaction. The total volume of the reaction solution was 200 μL. The value of A340 was recorded by infinite M200 Microplate Reader (Tecan, Switzerland) at 1 min intervals for 5 min. The variations of absorbance of CDNB-binding insecticides were used to calculate the relative inhibition rate of different insecticides against recombinant GSTs *in vitro*. The inactivated recombinant GSTs protein was used as a negative control, while GTX was used as a positive control. Each of these assays was performed three times.

The median inhibition concentration (IC$_{50}$) was measured using different concentrations of TFP. Briefly, different concentrations of TFP were mixed with recombinant PxGSTσ and CDNB, and then incubated with 1 mM GSH under the same conditions described above to activate the reaction. The remaining activity of PxGSTσ was monitored using the above method. Relative inhibition was calculated using the formula (1):

$$\text{Relative inhibition}\,(\%) = \frac{\Delta OD340c - \Delta OD340t}{\Delta OD340c} \times 100 \quad (1)$$

(ΔOD340c, variation OD$_{340}$ of control group during 5 min; ΔOD340t, the variation OD$_{340}$ of treatment group during 5 min). Data were plotted into prism using Prism 6.0 software (GraphPad) to determine the value of IC$_{50}$.

2.12 Metabolism assays

In order to determine whether PxGSTs metabolize TFP, ultra high performance liquid chromatography (UPLC) (Shimadzu, Japan) was employed in the metabolism test. The metabolic assay followed the method of Wang *et al*. with a slight modification.[47] TFP was dissolved in acetone as a stock solution of 100 mM. The stock solution was diluted in sodium phosphate buffer (PBS) (50 mM, pH 7.4) to obtain 0.5 mM working solution for lateral assays. The metabolic reaction was carried out in a glass test tube. One milliliter TFP working solution was incubated with 1 mL recombinant PxGSTs protein dilution (containing 50 μg recombinant protein) initially for 10 min at 30 °C, then adding a final of concentration of 5 mM GSH (dissolved in previously described PBS buffer) to start the reaction; each assay was replicated three times. In the control groups 1 mL recombinant PxGSTs was replaced by 1 mL heat-inactive protein, with assays replicated

three times. The above mixture was incubated at 30 °C for 2 h with shaking at 200 rpm. Then 500 μL methanol (HPLC-grade) was added to the test tube, reacting with the aforementioned mixtures for 5 min to terminate the reaction. After that, the reaction solution was centrifuged at 13 000 rpm for 15 min at room temperature, using a 0.22-μm filter to transfer 1 mL supernatant to sample vials for UPLC detection. Reversed-phase HPLC was performed on a C18 column (3 μm, 2.1 × 100 mm, Shimadzu). Meanwhile, 80% methanol along with 20% water was used as the mobile phase to separate TFP at a flow rate of 0.8 mL min^{-1}, with a monitoring absorbance wavelength of 254 nm at 30 °C. The standard TFP was applied to localize the peak of TFP following the above-mentioned chromatographic conditions. The depletion rate was calculated by the formula (2).

Depletion of TFP (%)

$$= \frac{\text{Peak area (control group)} - \text{Peak area (treatment group)}}{\text{Peak area (control group)}} \times 100 \ (2).$$

The metabolism assays using native and mutant PxGSTs were all performed in a similar way. Data were analyzed by ANOVA with Tukey's multiple comparisons test.

3 RESULTS AND DISCUSSION

3.1 Toxicity determination of TFP to *P. xylostella*

Tolfenpyrad is an inhibitor of mitochondrial complex I electron transport with contact and stomach insecticidal activity against many pests, especially those like *P. xylostella*.[9,10] In this study, we used a leaf-dipping method to examine the stomach poison activity of TFP to *P. xylostella* larvae. The values of LC$_{10}$, LC$_{50}$ and LC$_{90}$ decreased gradually as the larvae were exposed to TFP over time (24–72 h). The value of LC$_{10}$, LC$_{50}$ and LC$_{90}$ of TFP against *P. xylostella* were 4.34, 15.8 and 43.28 mg L^{-1} at 48 h, respectively (Table 1). The mortality of the control group was <10%, suggesting that the bioassay method was valid. This result revealed that the insecticidal activity of TFP on *P. xylostella* was consistent with previous results.[11] Meanwhile, results of the bioassay demonstrate that our method is capable of inducing mortality and the determination of LC$_{10}$ (at 48 h) for the expression profile experiment.

3.2 Expression profiles of PxGSTs exposure to TFP

Insect GSTs play an important role in the intracellular transport of substances, the biosynthesis of pheromones, and a series of physiological and biochemical processes that protect the body from oxidative stress.[48–50] The upregulation of GST gene expression resulted from insecticide exposure induction may be related to detoxification of insecticides.[14] Here, the 3rd instar larvae of *P. xylostella* were exposed to the LC$_{10}$ concentration (4.34 mg L^{-1}) of TFP and the expression level of PxGSTs genes in larvae were

monitored within 48 h. The results show that the expression of the PxGST (δ, ε and σ) gene in *P. xylostella* increased first and then decreased after exposure to low concentrations of TFP. Among them, the expression level of PxGSTσ underwent the most obvious change. After being exposed to TFP for 3 h, PxGSTσ increased 1.88-fold and PxGSTδ increased 1.55-fold, respectively (Fig. 1). Then, the increase in PxGSTσ, PxGSTδ and PxGSTε gene expression levels decreased progressively after TFP treatment for 12 h. (Fig. 1).

The GST-mediated insecticide resistance was related mainly to the overexpression of GST.[29] Previous reports have shown that alteration of GSTs activity and GSTs gene expression level were relevant to the resistance to organophosphates, pyrethroid and benzoylureas in insects.[51–53] Likewise, the expression of insect GSTs can be induced by insecticides. Previous reports have suggested that insect δ and ε classes of GST can be upregulated by organophosphates and pyrethroids, indicating the involvement of GSTs in the detoxification of these insecticides.[54–56] For example, the 2.63- and 2.85-fold upregulation of BdGSTδ1 and BdGSTδ10 (respectively) were discovered in *Bactrocera dorsalis* exposing to malathion, suggesting the importance of BdGSTδ1 and BdGSTδ10 in malathion detoxification.[57] Under LC$_{10}$ concentrations of fenpropathrin, six GST genes of *Panonychus citri* showed time-dependent increases, indicating the transcriptional upregulation of GST genes might be one of the mechanisms for this acaricide detoxification.[58] Our findings displayed that expression profiles of PxGSTσ and PxGSTδ under TFP exposure were congruent with previous reports that insect GSTs were involved in insecticide detoxification. Thus, we infer that after contacting with TFP, the *P. xylostella* larvae respond to this adversity rapidly, upregulating the expression level of PxGSTs involved in TFP resistance. When the PxGSTs enzyme activity reached a certain level, the upregulating trend would decrease progressively. Based on the PxGSTs changing trends in response to TFP (Fig. 1), it is reasonable to speculate that PxGSTσ and PxGSTδ may play pivotal roles in the direct detoxification of TFP.

3.3 Recombinant protein expression and kinetics of PxGSTs

The recombinant PxGSTs proteins were obtained using a prokaryotic expression system in this study. As shown in Fig. S1, all three PxGSTs were highly expressed as soluble proteins in *E. coli* BL21 (DE3). The expected molecular weights of recombinant PxGSTσ, PxGSTδ and PxGSTε proteins were *c.* 25 kDa (Fig. S1) including *pET-30a* (+) vector tags. The production of purified proteins was *c.* 0.5 μg μL^{-1}.

As mentioned earlier, the detoxification function of GSTs can be attributed mainly to the catalysis of GSH binding to toxins.[59] In this study, the activity of PxGST proteins was measured by using CDNB as a substrate, with the concentration of GSH being fixed. According to the Michaelis–Menten plots, the values of K_m and V_{max} in PxGSTσ, PxGSTδ and PxGSTε were determined (Fig. S2).

Time(h)	Slope ± SE	LC$_{10}$ (95% confidence interval) mg L^{-1}	LC$_{50}$ (95% confidence interval) mg L^{-1}	LC$_{90}$ (95% confidence interval) mg L^{-1}	χ^2
24	2.53 ± 0.19	8.13(6.13–10.27)	22.13(18.71–28.49)	76.71(69.56–87.21)	6.24
48	1.79 ± 0.22	4.34(2.45–6.77)	15.8(10.65–21.34)	43.28(37.69–50.80)	7.63
72	2.64 ± 0.25	2.17(1.58–3.14)	6.04(3.22–10.03)	28.42(22.06–36.53)	10.82

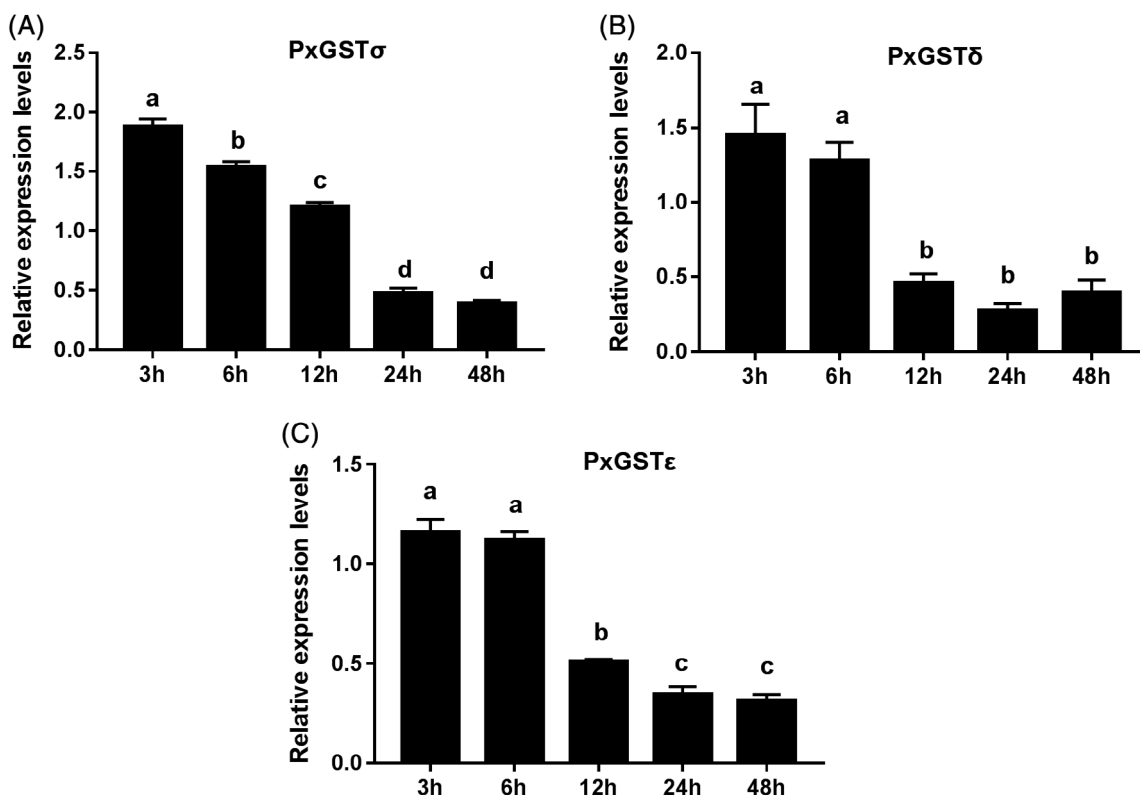**Table 1** Toxicity of TFP against *P. xylostella* over different times

Figure 1 Expression profiles of PxGSTx after LC_{10} TFP treatment at different time: (A) PxGSTσ, (B) PxGSTδ and (C) PxGSTε. Bars represent the mean ± SE of replicates. Different letters above error bars represent significant differences ($P < 0.05$) using one-way ANOVA followed by Tukey's multiple comparison tests.

The values of K_m and V_{max} were comparable to the reported enzyme kinetic characteristics of other insect recombinant GSTs proteins.[22,60,61] The catalytic efficiency (K_{cat} / K_m) of PxGSTσ, PxGSTδ and PxGSTε were 2.68×10^5 min^{-1} mM^{-1}, 8.14×10^5 min^{-1} mM^{-1} and 5.28×10^4 min^{-1} mM^{-1}, respectively. This illustrated that PxGSTs proteins had satisfactory binding affinity to CDNB (Fig. S2).

3.4 Inhibition of PxGSTs by insecticides *in vitro*

Glutathione S-transferases catalyze the conjugation of GSH with other compounds. Thus the inhibitory effect of insecticides on GSTs can reflect the affinity of GSTs to insecticides, which is used to indicate whether GSTs are directly involved in the metabolism of pesticides.[47] The inhibitory effect of insecticides on GSTs is manifested by reducing the rate of GSTs in catalyzing the reaction of GSH and CDNB. Studies have described that insecticides, such as chlorpyrifos, malathion, phoxim, permethrin and deltamethrin,[62,63] have inhibitory activities against insect GSTs *in vitro*. In this study, *in vitro* inhibition assays were performed on PxGSTs (PxGSTσ, PxGSTδ, PxGSTε) by using imidacloprid, thiamethoxam, rotenone, halofenozide, (E)-fenpyroximate, chlorantraniliprole, diflubenzuron and the positive inhibitor S-hexyl glutathione (GTX).

The results uncovered that no test insecticides but TFP and GTX exhibit significant inhibitory effects on the binding of CDNB to PxGSTs (Table S2). The inhibition rates of 500 μM TFP on PxGSTσ, PxGSTδ and PxGSTε were 70.68%, 37.91% and 36.51%, respectively. Even lower concentrations (20 μM and 100 μM) of TFP also had a certain inhibitory effect on PxGSTσ (22.32% and 48.15%). However, at the concentration of 20 μM, TFP had little inhibitory

effect on PxGSTδ and PxGSTε (Table S2). Because the water solubility of TFP is relatively low, it cannot be configured in a larger concentration. Hence, this experiment only determined the IC_{50} of TFP against PxGST σ inhibition activity, and its IC_{50} value was 114.50 μM (Fig. S3).

Previous studies suggested that the inhibition of insecticides on insect GSTs was associated with insecticide detoxification metabolism.[64] For example, the four GSTs of *Anopheles dirus* were inhibited by many insecticides, suggesting AdGSTs were correlated with insecticide detoxification.[65] The GSTs of *Liposcelis bostrychophila* were inhibited by carbosulfan, β-cypermethrin and chlorpyrifos, implying that GSTs were associated with insecticide detoxification.[66] In our study, TFP was capable of inhibiting the three classes of PxGSTs, with a particularly strong inhibitory effect on PxGSTσ (IC_{50} = 114.50 μM). This implied that TFP had a better affinity towards PxGSTs than the substrate CDNB, thus inhibiting the conjugation reaction between GSH and CDNB calalyzed by PxGSTs. Therefore, we infer that the strong binding capability of TFP towards PxGSTs is key evidence that PxGSTs are responsible for TFP detoxification.

3.5 Metabolism of TFP by PxGSTs

In order to explore the function of PxGSTs further, the metabolic effect of purified PxGSTs protein on TFP (0.5 mM) was examined by UPLC assay in the present study. The results show that PxGSTσ metabolized 26.38% of TFP in the 2-h reaction. The metabolism ability of PxGSTδ, metabolizing 11.51% TFP, was close to half of that of PxGSTσ, but PxGSTε hardly metabolized TFP (Fig. 2).

Insect GSTs are widely known to be phase II detoxification enzymes in insects. As reported, insect GSTs are able to detoxify
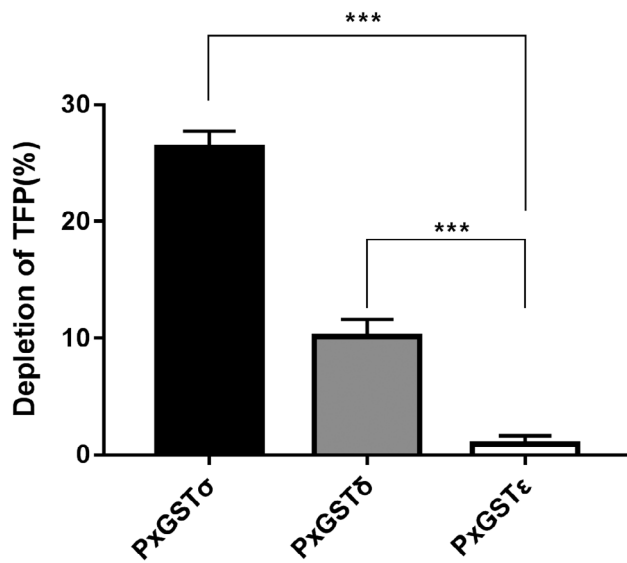
Figure 2 Metabolic capacity of three classes of PxGSTs toward TFP (0.5 mM). Metabolic capacity was shown as depletion of TFP (%). Bars represent the mean ± SE of replicates. Asterisks represent statistically significant differences analyzed by the one-way ANOVA with Tukey's multiple comparison tests (***, $P < 0.001$).

insecticides mainly via the dehydrochlorination reaction, peroxidase activity and sequestration.[20] Based on previous studies, insect GSTs were found to be likely to metabolize pyrethroids and organophosphates insecticides directly.[18] For example, HaGST-8 of *Helicoverpa armigera* had the capacity of metabolizing chlorpyrifos and cypermethrin.[67] Additionally, it was reported that one of the δ class GST in *Culex pipiens* was able to metabolize dichlorodiphenyltrichloroethane (DDT).[68] TuGSTδ05 in *Tetranychus urticae* was associated with metabolizing cyflumetofen directly.[69] Furthermore, according to earlier research, the insecticides that can be metabolized by GSTs usually possess the ability to inhibit the activity of corresponding GSTs. Taking lambda-cyhalothrin for example, it is reported to be metabolized by three GSTs from *Cydia pomonella* (CpGSTδ1, CpGSTδ3 and CpGSTε3). Meanwhile, lambda-cyhalothrin exhibited inhibitory effects on the activity of these three CpGSTs.[23,47,70] Moreover, insect GSTs could not only be inhibited by DDT, but also be metabolized by DDT.[71,72] It seems that the high affinity between insecticides and GSTs guarantees the high efficiency of GSTs in metabolizing certain insecticides. In our study, a similar phenomenon was found in the metabolism of TFP by PxGSTs. TFP had a stronger inhibitory effect on PxGSTσ, and PxGSTσ could metabolize TFP effectively. Furthermore, the inhibitory effect of TFP on PxGSTδ was weaker than PxGSTσ and the metabolic capacity of PxGSTδ also was weaker. Therefore, we infer that among the three classes of PxGSTs, PxGSTσ was superior in metabolizing TFP. Moreover, PxGSTσ displayed a strong binding affinity towards TFP, such sequestration may be involved in TFP detoxification.

3.6 Binding mode analysis

The accurate binding mode of PxGSTσ–TFP was obtained by performing molecular docking in GOLD 5.3. The best model of the PxGSTσ–TFP complex [Fig. 3(A)] was subjected to Chemscore function in Amber 12, and the calculated binding free energy (ΔG_{cal}) was estimated to be −7.31 kcal mol^{-1} (Table 2). Based on the IC$_{50}$ values of TFP against PxGSTσ, the experimental binding
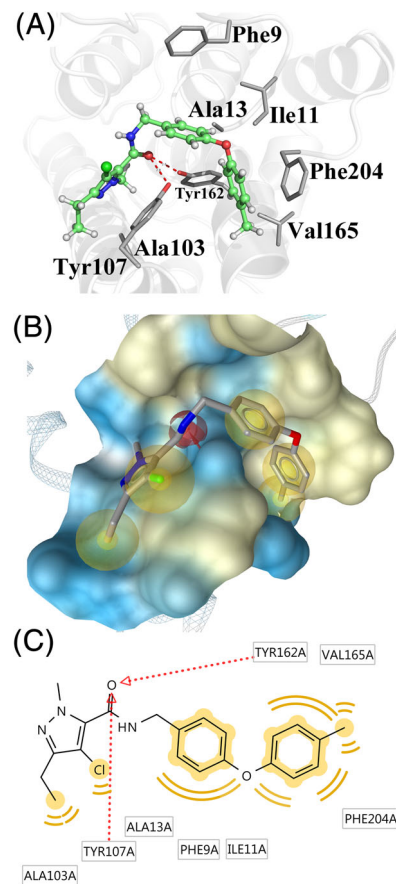

Figure 3 (A) The binding mode of the PxGSTσ–TFP complex produced by molecule docking analysis. TFP is presented with the stick-and-sphere model. Color code: green, C; deep green, Cl; blue, N; red, O; white, H. Key residues are presented with the stick model. Color code: gray, C; red, O; white, H; red-dashed line, H-bond. (B) The pharmacophore model derived from the binding mode of the PxGSTσ–TFP complex. The pharmacophore model consists of four hydrophobic features (yellow sphere), and two H-bond acceptors (red arrow and red sphere). (C) The 2D interaction diagram of the PxGSTσ–TFP complex. The 2D interaction diagram of TFP with PxGSTσ were visualized with the following color code: H-bond acceptor (red arrow), and hydrophobic interaction (yellow sphere).

free energy (ΔG_{exp}) of the PxGSTσ–TFP complex was calculated to be −5.41 kcal mol^{-1}.[73] The values of ΔG_{cal} and ΔG_{exp} were qualitatively in agreement with the difference being not beyond 2.00 kcal mol^{-1}, further suggesting the reliability of the PxGSTσ–TFP complex model obtained through molecular docking.

As shown in Fig. 3(A), the molecule TFP was located in the hydrophobic pocket composed of residues including Phe9, Ile11, Ala13, Ala103, Tyr107, Tyr162, Val165 and Phe204. To figure out the interaction modes between the groups of TFP and the binding pocket of PxGSTσ, a pharmacophore model derived from the PxGSTσ–TFP interactions was generated [Fig. 3(B)]. In the pharmacophore model, the yellow sphere represents the hydrophobic feature, and the red sphere plus red arrow represents the feature of H-bond donor. In the 2D diagram of the pharmacophore model [Fig. 3(C)], it is clear that the ethyl and C1 derived from the pyrazol group of TFP formed hydrophobic interactions with Ala13, Ala103 and Try107. Hydrophobic interactions also were detected at the sites between phenoxyl and PxGSTσ residues (Phe9, Ala13 and Ile11). Another hydrophobic interaction occurred between the TFP cresyl group and PxGSTσ. In detail,

Table 2 The calculated and experimental binding free energy* for the binding of TFP to PxGSTσ

Name	Structure	S(h-bond)	S(lipo)	H(rot)	ΔG_{cal}†	ΔG_{exp}‡
TFP		0.27	239.65	1.49	−7.31	−5.41

*All binding free energy values are given in kcal mol^{-1}.
†ΔG_{cal} represents calculated binding free energy.
‡ΔG_{exp} represents experimental binding free energy.

the methyl of TFP cresyl interacted dominantly with Val165 and Phe204 in the hydrophobic form, and the benzene ring of TFP cresyl formed hydrophobic interactions with Ile11, Tyr162, Val165 and Phe204, simultaneously. Besides hydrophobic interactions, other forms of interaction also were observed. The cresyl of TFP also interacted with the sidechains of Phe9 (phenyl and phenoxyl) and Phe204 (phenyl) through π-stacking interactions. The O atom derived from the amide group of TFP could form H-bond interactions with Tyr107 and Tyr162 simultaneously (Fig. 3), with the distances between hydrogen binding atoms being 2.8 Å and 2.6 Å [Fig. 3(A)].

Based on the interactions between PxGSTσ and TFP, we speculate that in the metabolizing process of TFP by PxGSTσ, the hydrophobic interactions mentioned above together with the π-stacking interactions hold TFP into the hydrophobic pockets of PxGSTσ tightly. Considering the role of nucleophilic attack in the metabolizing process, the H-bonds provided by Tyr107 and Tyr162 may be critical to the detoxification of TFP. To verify the assumption, Tyr107 and Tyr162 were individually mutated into Ala in the subsequent research.

3.7 Site-directed mutagenesis and metabolism assay
The key residues (Tyr107 and Tyr 162) of PxGSTσ derived from the prediction of binding model were mutated into Ala by site-directed mutagenesis. The expected molecular weights of 25 kDa mutant proteins were obtained by prokaryotic expression (Fig. S1). As presented in the Michaelis–Menten plots, the values of V_{max} and K_m in PxGSTσY107A and PxGSTσY162A were 241.7 ± 3.25 μм$^{-1}$mg^{-1}min^{-1}, 232.9 ± 3.82 μм$^{-1}$ mg^{-1} min^{-1} and 0.18 ± 0.0074 mм, 0.16 ± 0.0098 mм, respectively (Fig. S2). The kinetic parameters of the mutant PxGSTσ proteins displayed no significant differences with their native counterpart, implying that the mutants were applicable to the subsequent experiments.

In vitro inhibition assay of TFP on the two mutant proteins showed that the inhibition rates were 15.24 ± 3.25% (PxGSTσY107A) and 10.25 ± 4.28% (PxGSTσY162A) under 100 μм of TFP. When the TFP concentration reached 500 μм, its inhibition rates on the two variants, 26.85 ± 3.97% and 25.34 ± 3.66%, remained much lower than on the native form (Fig. 4). Results derived from UPLC assay indicate that the two mutant proteins metabolized 10.59% and 8.71% of TFP in 2 h, respectively (Fig. 5).

The above results illustrate that mutant PxGSTσY107A and PxGSTσY162A proteins almost lost binding and had a significantly decreased ability to metabolize TFP. This confirms our hypothesis that the H-bonds from Tyr107 and Tyr162 are crucial for TFP detoxification. When the two sites mutated to alanine, the O-atom of the amide group served by TFP was unable to interact with Tyr107 and Tyr162 to form H-bonds. The hydrophobic
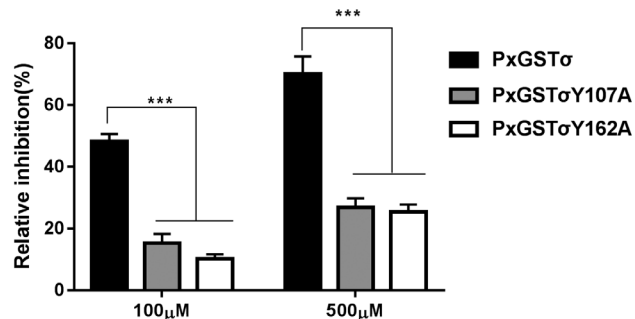

Figure 4 Inhibition of TFP on PxGSTσ and its mutant protein: PxGSTσY107A and PxGSTσY162A (standing for the PxGSTσ proteins mutated at the sites of Tyr107 and Tyr162). Bars represent the mean ± SE of replicates. Asterisks represent statistically significant differences analyzed by the one-way ANOVA with Tukey's multiple comparison tests (***, $P < 0.001$).
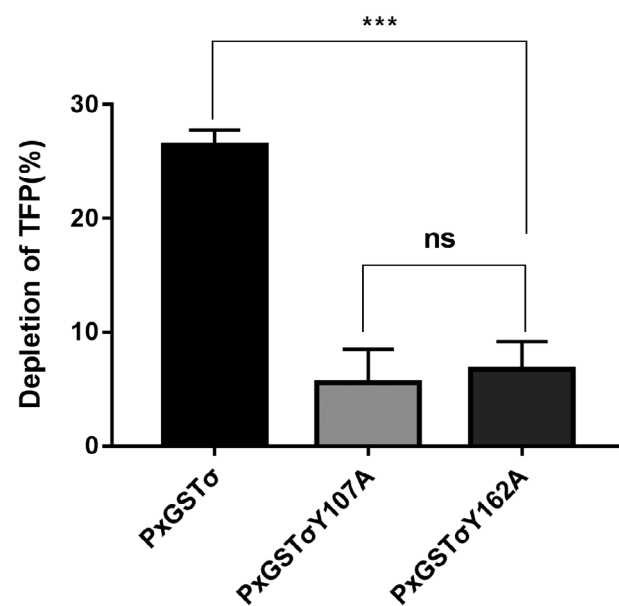

Figure 5 Metabolic capacity of PxGSTσ and its mutants (PxGSTσY107A and PxGSTσY162A) towards TFP. PxGSTσY107A and PxGSTσY162A stand for the PxGSTσ proteins mutated at the sites of Tyr107 and Tyr162. Metabolic capacity was shown as depletion of TFP (%) (Bars represent the mean ± SE of replicates. Asterisks represent statistically significant differences analyzed by the one-way ANOVA with Tukey's multiple comparison tests (***, $P < 0.001$, ns: no significance.).

interactions between TFP (ethyl and C1 of the pyrazol group) and Try107 along with the hydrophobic interaction that occurred between the TFP cresyl group and Tyr162 were broken. Thus, the

mutant proteins PxGSTσY107A and PxGSTσY162A cannot metabolize TFP.

4 CONCLUSION

Overall, the above findings illustrate that PxGSTσ, PxGSTδ and PxGSTε are involved in detoxifying TFP in *P. xylostella*. Of the three PxGSTs, PxGSTσ is equipped with the highest binding and metabolic capacities towards TFP. Furthermore, the binding modes of PxGSTσ–TFP interaction and the key residues (Tyr107 and Tyr162) involved are revealed. This study illuminates the molecular mechanism of PxGSTσ in metabolizing TFP, and lays a foundation for the design and optimization of TFP-like compounds.

AUTHOR CONTRIBUTIONS

YLZ and JYL conceived the project; JYL and YFL designed the experiment; YFL, HS, TZ, XXS, YL, XY, YFZ and SLZ performed the experiments and prepared the manuscript; and YLZ and JYL supervised the study and contributed reagents/materials. All authors contributed to data analysis.

CONFLICT OF INTERESTS

The authors declare no competing financial interest.

SUPPORTING INFORMATION

Supporting information may be found in the online version of this article.

REFERENCES

1 Vaschetto LM and Beccacece HM, The emerging importance of noncoding RNAs in the insecticide tolerance, with special emphasis on *Plutella xylostella* (Lepidoptera: Plutellidae). *WIREs RNA* **10**:e1539 (2019).

2 Talekar NS and Shelton AM, Biology, ecology, and management of the diamondback moth. *Annu Rev Entomol* **38**:275–301 (1993).

3 Zalucki MP, Shabbir A, Silva R, Adamson D, Liu SS and Furlong MJ, Estimating the economic cost of one of the world's major insect pests, *Plutella xylostella* (Lepidoptera: Plutellidae): just how long is a piece of string? *J Econ Entomol* **105**:1115–1129 (2012).

4 Mazhawidza E and Mvumi BM, Field evaluation of aqueous indigenous plant extracts against the diamondback moth, *Plutella xylostella* L. and the rape aphid, *Brevicoryne brassicae* L. in brassica production. *Ind Crop Prod* **110**:36–44 (2017).

5 Liao JY, Xue YQ, Xiao GJ, Xie M, Huang S, You S *et al.*, Inheritance and fitness costs of resistance to *Bacillus thuringiensis* toxin Cry2Ad in

laboratory strains of the diamondback moth, *Plutella xylostella* (L.). *Sci Rep* **9**:6113 (2019).

6 Li ZY, Feng X, Liu SS, You MS and Furlong MJ, Biology, ecology, and management of the diamondback moth in China. *Annu Rev Entomol* **61**:277–296 (2016).

7 Zhu B, Shan JQ, Li R, Liang P and Gao XW, Identification and RNAi-based function analysis of chitinase family genes in diamondback moth, *Plutella xylostella*. *Pest Manag Sci* **75**:1951–1961 (2019).

8 Lin QS, Jin FL, Hu ZD, Chen HY, Yin F, Li ZY *et al.*, Transcriptome analysis of chlorantraniliprole resistance development in the diamondback moth *Plutella xylostella*. *PLoS One* **8**:e72314 (2013).

9 Okada I, Okui S, Fukuchi T and Yoshiya K, Synthesis and insecticidal activity of N-(tolyloxybenzyl)-pyrazolecarboxamide derivatives. *J Pestic Sci* **24**:393–396 (1999).

10 Insecticide Resistance Action Committee (IRSA) 2019. https://www.irac-online.org/search/?k=Tolfenpyrad+ [18 September 2019].

11 Song HJ, Liu YX, Xiong LX, Li YQ, Yang N and Wang QM, Design, synthesis, and insecticidal activity of novel pyrazole derivatives containing alpha-hydroxymethyl-N-benzyl carboxamide, alpha-chloromethyl-N-benzyl carboxamide, and 4,5-dihydrooxazole moieties. *J Agric Food Chem* **60**:1470–1479 (2012).

12 Chen Q, Chen JQ, Huang SJ, Chen HF, Qin WJ and Qin HG, Realized heritability and risk assessment of resistance of *Plutella xylostella* to tolfenpyrad. *Jiangsu J Agric Sci* **31**:267–271 (2015).

13 Sukonthabhirom S and Siripontangmun S, Toxicity of insecticides on diamondback moth from three areas in Thailand, in Proceedings of SEAVEG 2012: High Value Vegetables in Southeast Asia: Production, Supply and Demand, ed. by Holmer R, Linwattana G, Nath P and Keatinge JDH. Chiang Mai. AVRDC-The World Vegetable Center, pp. 97–103 (2013).

14 Li XC, Schuler MA and Berenbaum MR, Molecular mechanisms of metabolic resistance to synthetic and natural xenobiotics. *Annu Rev Entomol* **52**:231–253 (2007).

15 Etebari K, Afrad MH, Tang B, Silva R, Furlong MJ and Asgari S, Involvement of microRNA miR-2b-3p in regulation of metabolic resistance to insecticides in *Plutella xylostella*. *Insect Mol Biol* **27**:478–491 (2018).

16 Ranson H and Hemingway J, Mosquito glutathione transferases. *Methods Enzymol* **401**:226–241 (2005).

17 Kostaropoulos I, Mantzari AE and Papadopoulos AI, Alterations of some glutathione S-transferase characteristics during the development of *Tenebrio molitor* (Insecta:Coleoptera). *Insect Biochem Mol Biol* **26**:963–969 (1996).

18 Enayati AA, Ranson H and Hemingway J, Insect glutathione transferases and insecticide resistance. *Insect Mol Biol* **14**:3–8 (2005).

19 Kostaropoulos I, Papadopoulos AI, Metaxakis A, Boukouvala E and Papadopoulou-Mourkidouet E, The role of glutathione S-transferases in the detoxification of some organophosphorus insecticides in larvae and pupae of the yellow mealworm, *Tenebrio molitor* (Coleoptera: Tenebrionidae). *Pest Manag Sci* **57**:501–508 (2001).

20 Pavlidi N, Vontas J and Van Leeuwen, the role of glutathione S-transferases (GSTs) in insecticide resistance in crop pests and disease vectors. *Curr Opin Insect Sci* **27**:97–102 (2018).

21 Balakrishnan B, Su S, Zhang CH and Chen MH, Identification and functional characterization of two sigma glutathione S-transferase genes from bird cherry-oat aphid (Hemiptera: Aphididae). *J Econ Entomol* **112**:416–424 (2019).

22 Zhou L, Fang SM, Huang K, Yu QY and Zhang Z, Characterization of an epsilon-class glutathione S-transferase involved in tolerance in the silkworm larvae after long term exposure to insecticides. *Ecotox Environ Safe* **120**:20–26 (2015).

23 Liu JY, Yang XQ and Zhang YL, Characterization of a lambda-cyhalothrin metabolizing glutathione S-transferase *CpGSTd1* from *Cydia pomonella* (L.). *Appl Microbiol Biotechnol* **98**:8947–8962 (2014).

24 Chelvanayagam G, Parker MW and Board PG, Fly fishing for GSTs: a unified nomenclature for mammalian and insect glutathione transferases. *Chem Biol Interact* **133**:256–260 (2001).

25 Friedman R, Genomic organization of the glutathione S-transferase family in insects. *Mol Phylogenet Evol* **61**:924–932 (2011).

26 You YC, Xie M, Ren NN, Cheng XM, Li JY, Ma XL *et al.*, Characterization and expression profiling of glutathione S-transferases in the diamondback moth, *Plutella xylostella* (L.). *BMC Genomics* **16**: 13 (2015).

27 Liu JY, Li YF, Tian Z, Sun H, Chen XE, Zheng SL *et al.*, Identification of key residues associated with the interaction between *Plutella xylostella*

sigma-class glutathione S-transferase and the inhibitor s-hexyl glutathione. *J Agric Food Chem* **66**:10169–10178 (2018).

28 Ranson H, Claudianos C, Ortelli F, Abgrall C, Hemingway J, Sharakhova MV *et al.*, Evolution of supergene families associated with insecticide resistance. *Science* **298**:179–181 (2002).

29 Ranson H, Rossiter L, Ortelli F, Jensen B, Wang XL, Roth CW *et al.*, Identification of a novel class of insect glutathione S-transferases involved in resistance to DDT in the malaria vector *Anopheles gambiae*. *Biochem J* **359**:295–304 (2001).

30 Yu XL, Sun RJ, Yan HR, Guo XQ and Xu BH, Characterization of a sigma class glutathione S-transferase gene in the larvae of the honeybee (*Apis cerana cerana*) on exposure to mercury. *Comp Biochem Physiol B Biochem Mol Biol* **161**:356–364 (2012).

31 Sue M and Yajima S, Crystal structure of the delta-class glutathione transferase in *Musca domestica*. *Biochem Biophys Res Commun* **502**: 345–350 (2018).

32 Okada I, Okui S, Wada M and Takahashi Y, Synthesis and insecticidal activity of N-(4-aryloxybenzyl)-pyrazolecarboxamide derivatives. *J Pestic Sci* **21**:305–310 (1996).

33 Abbott WS, A method of computing the effectiveness of an insecticide. *J Econ Entomol* **18**:265–267 (1925).

34 Fu W, Xie W, Zhang Z, Wang SL, Wu QJ, Liu Y *et al.*, Exploring valid reference genes for quantitative real-time PCR analysis in *Plutella xylostella* (Lepidoptera: Plutellidae). *Int J Biol Sci* **9**:792–802 (2013).

35 Livak KJ, Analysis of relative gene expression data using real-time quantitative PCR and the $2^{-\Delta\Delta CT}$ method. *Methods* **25**:402–408 (2001).

36 Jones G, Willett P and Glen RC, Molecular recognition of receptor sites using a genetic algorithm with a description of desolvation. *J Mol Biol* **245**:43–53 (1995).

37 Jones G, Willett P, Glen RC, Leach AR and Taylor R, Development and validation of a genetic algorithm for flexible docking. *J Mol Biol* **267**:727–748 (1997).

38 Case D, Darden T, Cheatham T, Simmerling C, Wang J, Duke R *et al.*, *AMBER 12*. University of California, San Francisco, CA, USA (2012).

39 Hummer G, Rasaiah JC and Noworyta JP, Water conduction through the hydrophobic channel of a carbon nanotube. *Nature* **414**:188–190 (2001).

40 Wang J, Wolf RM, Caldwell JW, Kollman PA and Case DA, Development and testing of a general amber force field. *J Comput Chem* **25**:1157–1174 (2004).

41 Yang XQ, Liu JY, Li XC, Chen MH and Zhang YL, Key amino acid associated with acephate detoxification by *Cydia pomonella* carboxylesterase based on molecular dynamics with alanine scanning and site-directed mutagenesis. *J Chem Inf Model* **54**:1356–1370 (2014).

42 Chen XE, Liu JY and Zhang YL, Cantharidin impedes the activity of protein serine/threonine phosphatase in *Plutella xylostella*. *Mol Biosyst* **10**:240–250 (2014).

43 Wolber G and Langer T, LigandScout: 3-D pharmacophores derived from protein-bound ligands and their use as virtual screening filters. *J Chem Inf Model* **45**:160–169 (2005).

44 DeLano WL, The PyMOL molecular graphics system, version 1.3.0.4. *Schrödinger, LLC*. 2002.

45 Baxter CA, Murray CW, Clark DE, Westhead DR and Eldridge MD, Flexible docking using Tabu search and an empirical estimate of binding affinity. *Proteins* **33**:367–382 (1998).

46 Eldridge MD, Murray CW, Auton TR, Paolini GV and Mee RP, Empirical scoring functions: I. the development of a fast empirical scoring function to estimate the binding affinity of ligands in receptor complexes. *J Comput Aided Mol Des* **11**:425–445 (1997).

47 Wang W, Hu C, Li XR, Wang XQ and Yang XQ, *CpGSTd3* is a lambda-cyhalothrin metabolizing glutathione S-transferase from *Cydia pomonella* (L.). *J Agric Food Chem* **67**:1165–1172 (2019).

48 Ketterman AJ, Saisawang C and Wongsantichon J, Insect glutathione transferases. *Drug Metab Rev* **43**:253–265 (2011).

49 Pal R, Sanil N and Clark A, Developmental studies on the sigma and delta-1 glutathione transferases of *Lucilia cuprina*. *Comp Biochem Physiol D Genomics Proteomics* **7**:28–34 (2012).

50 Pavlidi N, Vontas J and Van Leeuwen T, The role of glutathione S-transferases (GSTs) in insecticide resistance in crop pests and disease vectors. *Curr Opin Insect Sci* **27**:97–102 (2018).

51 Qin GH, Liu T, Guo YP, Zhang XY, Ma EB and Zhang JZ, Effects of chlorpyrifos on glutathione S-transferase in migratory locust, Locusta Migratoria. *Pestic Biochem Physiol* **109**:1–5 (2014).

52 Lin YH, Lee CM, Huang JH and Lee HJ, Circadian regulation of permethrin susceptibility by glutathione S-transferase (*BgGSTD1*) in the German cockroach (*Blattella germanica*). *J Insect Physiol* **65**:45–50 (2014).

53 Sonoda S and Tsumuki H, Studies on glutathione S-transferase gene involved in chlorfluazuron resistance of the diamondback moth, *Plutella xylostella* L. (Lepidoptera: Yponomeutidae). *Pestic Biochem Physiol* **82**:94–101 (2005).

54 Lumjuan N, Rajatileka S, Changsom D, Wicheer J, Leelapat P, Prapanthadara LA *et al.*, The role of the *Aedes aegypti* epsilon glutathione transferases in conferring resistance to DDT and pyrethroid insecticides. *Insect Biochem Mol Biol* **41**:203–209 (2001).

55 Low WY, Feil SC, Ng HL, Gorman MA, Morton CJ, Pyke J *et al.*, Recognition and detoxification of the insecticide DDT by *Drosophila melanogaster* glutathione S-transferase D1. *J Mol Biol* **399**:358–366 (2010).

56 Kostaropoulos I, Papadopoulos AI, Metaxakis A, Boukouvala E and Papadopoulou-Mourkidou E, Glutathione S-transferase in the defence against pyrethroids in insects. *Insect Biochem Mol Biol* **31**: 313–319 (2001).

57 Meng LW, Yuan GR, Lu XP, Jing TX, Zheng LS, Yong HX *et al.*, Two delta class glutathione S-transferases involved in the detoxification of malathion in *Bactrocera dorsalis* (Hendel). *Pest Manag Sci* **75**:1527–1538 (2019).

58 Liao CY, Zhang K, Niu JZ, Ding TB, Zhong R, Xia WK *et al.*, Identification and characterization of seven glutathione S-transferase genes from citrus red mite, *Panonychus citri* (McGregor). *Int J Mol Sci* **14**:24255–24270 (2013).

59 Chen XE and Zhang YL, Identification and characterisation of multiple glutathione S-transferase genes from the diamondback moth, Plutella xylostella. *Pest Manag Sci* **71**:592–600 (2015).

60 Reid WR, Sun HN, Becnel JJ, Clark AG and Scott JG, Overexpression of a glutathione S-transferase (Mdgst) and a galactosyltransferase-like gene (Mdgt1) is responsible for imidacloprid resistance in house flies. *Pest Manag Sci* **75**:37–44 (2019).

61 Habig WH, Pabst MJ, Jakoby WB and S-transferases G, the first enzymatic step in mercapturic acid formation. *J Biol Chem* **249**:7130–7139 (1974).

62 Xu ZB, Zou XP, Zhang N, Feng QL and Zheng SC, Detoxification of insecticides, allechemicals and heavy metals by glutathione S-transferase SlGSTE1 in the gut of *Spodoptera litura*. *Insect Sci* **22**:503–511 (2015).

63 Wilding CS, Weetman D, Rippon EJ, Steen K, Mawejje H, Barsukov IL *et al.*, Parallel evolution or purifying selection, not introgression, explains similarity in the pyrethroid detoxification linked GSTE4 of *Anopheles gambiae* and *An. arabiensis*. *Mol Genet Genomics* **290**: 201–215 (2015).

64 Prapanthadara L, Ranson H, Somboon P and Hemingway J, Cloning, expression and characterization of an insect class I glutathione S-transferase from *Anopheles dirus* species B. *Insect Biochem Mol Biol* **28**:321–329 (1997).

65 Prapanthadara L, Promtet N, Koottathep S, Somboon P and Ketterman AJ, Isoenzymes of glutathione S-transferase from the mosquito *Anopheles dirus* species B: the purification, partial characterization and interaction with various insecticides. *Insect Biochem Mol Biol* **30**:395–403 (2000).

66 Dou W, Wu S, Hassan MW and Wang JJ, Purification and biochemical characterization of glutathione S-transferases from three strains of *Liposcelis bostrychophila* Badonnel (Psocoptera: Liposcelididae): implication of insecticide resistance. *Pestic Biochem Physiol* **94**:10–14 (2009).

67 Labade CP, Jadhav AR, Ahire M, Zinjarde SS and Tamhane VA, Role of induced glutathione-S-transferase from *Helicoverpa armigera*, (Lepidoptera: Noctuidae) HaGST-8 in detoxification of pesticides. *Ecotoxicol Environ Saf* **147**:612–621 (2018).

68 Samra AI, Kamita SG, Yao HW, Cornel AJ and Hammock BD, Cloning and characterization of two glutathione Stransferases from pyrethroid-resistant *Culex pipiens*. *Pest Manag Sci* **68**:764–772 (2012).

69 Pavlidi N, Khalighi M, Myridakis A, Dermauw W, Wybouw N, Tsakireli D *et al.*, A glutathione-S-transferase (TuGSTd05) associated with acaricide resistance in *Tetranychus urticae* directly metabolizes the

complex II inhibitor cyflumetofen. *Insect Biochem Mol Biol* **80**:101–115 (2017).

70 Hu C, Wang W, Ju D, Chen GM, Tan XL, Mota-Sanchez D *et al.*, Functional characterization of a novel λ-yhalothrin metabolising glutathione S-transferase, CpGSTe3, from the codling moth *Cydia pomonella. Pest Manag Sci* **76**:1039–1047 (2019).

71 Udomsinprasert R, Pongjaroenkit S, Wongsantichon J, Oakley AJ, Prapanthadara LA, Wilce M *et al.*, Identification, characterization and structure of a new Delta class glutathione transferase isoenzyme. *Biochem J* **388**:763–771 (2005).

72 Tang AH and Tu CP, Biochemical characterization of *Drosophila glutathione* S-transferases D1 and D21. *J Biol Chem* **269**:27876–27884 (1994).

73 Moreira IS, Fernandes PA and Ramos MJ, Computational alanine scanning mutagenesis—an improved methodological approach. *J Comput Chem* **28**:644–654 (2007).